The heavily polluted atmosphere of the DAZ white dwarf GALEX J193156.8+011745 *

S. Vennes¹†, A. Kawka¹‡, and P. Németh²§ ¹Astronomický ústav AV ČR, Fričova 298, CZ-251 65 Ondřejov, Czech Republic

- ² Department of Physics and Space Sciences, 150 W. University Blvd, Florida Institute of Technology, Melbourne, FL 32901, USA

ABSTRACT

We report on the discovery of a new heavily polluted white dwarf. The DAZ white dwarf GALEX J193156.8+011745 was identified in a joint GALEX/GSC survey of ultraviolet-excess objects. Optical spectra obtained at ESO NTT show strong absorption lines of magnesium and silicon and a detailed abundance analysis based on VLT-Kueyen UVES spectra reveal super-solar abundances of silicon and magnesium, and near-solar abundances of oxygen, calcium, and iron. The overall abundance pattern bears the signature of ongoing accretion onto the white dwarf atmosphere. The infrared spectral energy distribution shows an excess in the H and K bands likely associated with the accretion source.

Key words: stars: abundance - stars: individual: GALEX J193156.8+011745 - white dwarfs

INTRODUCTION

The GALEX J193156.8 + 011745(hereafter GALEX J1931+0117) is a hydrogen-rich white dwarf recently identified in a joint ultraviolet/optical survey (Vennes et al. 2010) based on the Galaxy Evolution Explorer (GALEX) all-sky survey¹ and the GSC2.3.2 catalogue. The Third U.S. Naval Observatory CCD Astrograph $Catalog^2$ locates the star at R.A.(2000) = 19 31 56.933, Dec.(2000) = +01 17 44.13 with a proper motion of $\mu_{\alpha} \cos \delta = -77.6 \pm 6.4 \text{ and } \mu_{\delta} = -6.1 \pm 6.1 \text{ mas yr}^{-1}.$ The distance modulus implies that the star is nearby $(\approx 55 \text{ pc})$ and that it is imbedded in the Galactic plane $(|z| \approx 8 \text{ pc})$. Based on echelle spectroscopy we show that GALEX J1931+0117 is a DAZ white dwarf and is one of the most extreme cases of externally polluted white dwarf atmospheres.

The DAZ white dwarf atmospheres are hydrogendominated with heavy element abundances ranging from nearly solar down to detection limits several orders of magnitude below solar (Zuckerman et al. 2003; Koester et al. 2005). The DAZ and, more particularly, the DZ phenom-

- E-mail: vennes@sunstel.asu.cas.cz
- E-mail: kawka@sunstel.asu.cas.cz
- Email: pnemeth@fit.edu

ena are interpreted as evidence of on-going accretion of circumstellar material onto white dwarf atmospheres (e.g., Kilic & Redfield 2007). The source of the material has been ascribed to comets (Alcock, Fristrom, & Siegelman 1986) and more recently to tidally-disrupted asteroids (see Jura 2008), although close, low-mass companions in post-common envelope binaries are also a known source of material (Debes 2006; Kawka et al. 2008).

The observational evidence in favour of the accretion of debris material resides in (1) the inferred composition of the accretion flow (Zuckerman et al. 2007) showing an overabundance of refractory elements (see a discussion on the solar system by Lodders 2003), and (2) the direct spectroscopic signature of gaseous discs as in the cases of SDSS J122859.93+104032.9and SDSS J104341.53+085558.2 (Gänsicke et al. 2006; Gänsicke, Marsh, & Southworth 2007) or dusty discs (e.g., Farihi, Jura, & Zuckerman 2009; Brinkworth et al. 2009).

The accreted material may also be supplied by mass loss from a close, low-mass, and possibly substellar companion. Only a few substellar companion to white dwarf stars are known such as the white dwarf plus L8-9 resolved pair PHL 5028 (Steele et al. 2009) or close DA plus L8 postcommon envelope binary WD0137-349 (Maxted et al. 2006; Burleigh et al. 2006). Relatively luminous DAZ white dwarfs such as EG 102 (Holberg, Barstow, & Green 1997) may hide low-mass companions, but Debes, Sigurdsson, & Woodgate (2005) limits them to substellar types. The mass loss material captured by the deep potential well of a white dwarf should reflect the composition of the chromosphere of the red dwarf, which, in most cases, should be close to solar.

^{*} Based on observations made with ESO telescopes at the La Silla Paranal Observatory under programmes 83.D-0540 and 283.D-

See Morrissey et al. (2007) for a description of the data prod-

² Accessed at VizieR (Ochsenbein, Bauer, & Marcout 2000).

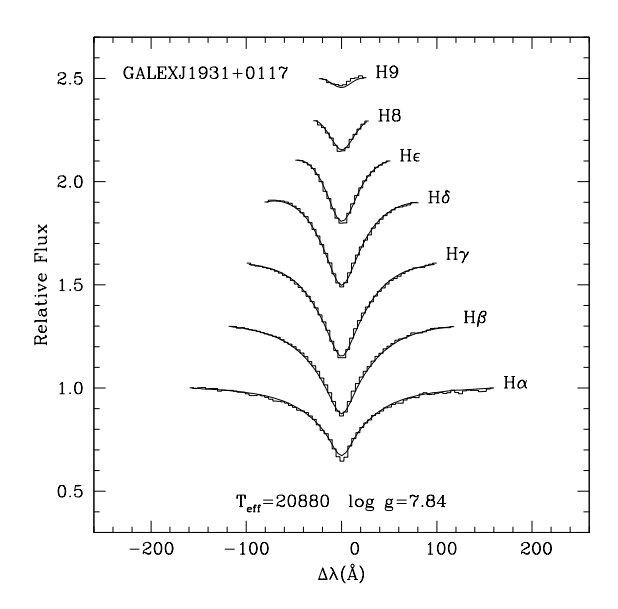


Figure 1. Model fits (solid lines) to the low dispersion (EFOSC2) Balmer line profiles (jagged lines) and best-fit parameter values $(T_{\rm eff}, \log g)$.

In this context, the discovery of the peculiar DAZ white dwarf GALEX J1931+0117 is timely. We present a series of ultraviolet (UV), optical and near infrared (NIR) observations (Section 2) and our model atmosphere analysis (Section 3.1) revealing a DAZ white dwarf with a peculiar abundance pattern (Section 3.2). A notable NIR excess (Section 3.3) may hold clues concerning the nature of this external source. We summarise and conclude in Section 4.

2 OBSERVATIONS

Vennes et al. (2010) describe a selection of hot sub-luminous stars in a joint GALEX/GSC2.3.2 survey. Briefly, a UV excess along with measurable proper-motion is interpreted as a likely, but not definitive, characteristic of hot subdwarfs (sdB, sdO) or white dwarfs. To confirm the selection, follow-up spectroscopy was done for a number of candidates including GALEX J1931+0117. We obtained two low-dispersion spectra ($t_{\rm exp}=600$ s) using EFOSC2 attached to the New Technology Telescope (NTT) at La Silla Observatory on UT 2009 August 25 (grating #11, dispersion = 4.15 Å pixel⁻¹). The spectral coverage is from 3680 to 7408Å at a resolution of ≈ 15.8 Å.

Following the identification of GALEX J1931+0117 as a DAZ white dwarf we obtained three echelle spectra ($t_{\rm exp}=1450$ s) using UVES attached to the VLT-Kueyen on UT 2009 November 12 (dispersion ~ 0.02 Å pixel⁻¹). The first two echelle spectra were obtained with the red arm and cover the ranges 5698-7532Å and 7660-9464Å. A third spectrum obtained with the blue arm covers the range 3757-4985Å.

We collected the JHK photometry from the 2MASS survey (Skrutskie et al. 2006) and the GALEX photometry, corrected for nonlinearity (Morrissey et al. 2007), from the GR4+5 release. Despite a reddening index of $E_{B-V}=0.4054$ (Schlegel, Finkbeiner, & Davis 1998) in the

Table 1. Photometry

Bandpass	Measurement		
GALEX FUV	13.20 ± 0.10		
GALEX NUV	13.55 ± 0.10		
V	14.20 ± 0.02		
2MASS J	14.66 ± 0.05		
2MASS H	14.55 ± 0.09		
2MASS~K	$14.45 {\pm} 0.10$		

line of sight toward GALEX J1931+0117, the star is relatively nearby and does not show the effect of reddening $(E_{B-V} \lesssim 0.01)$. Finally, we used the acquisition images (V filter) at NTT to measure the apparent magnitude of GALEX J1931+0117. We employed the acquisition images of the flux calibration standard Feige 110 (V = 11.832) and EG 21 (V = 11.40) obtained on the same night at the NTT to calibrate the measured counts and derive the V magnitudes. Table 1 summarises the available photometric measurements. The field surrounding GALEX J1931+0117 is somewhat crowded with objects 4.8 and 8.3" away. These separations are sufficient to exclude significant flux contamination in the optical and infrared images. The ultraviolet (FUV and NUV) images are possibly contaminated. However, the optical/infrared indices imply that the nearby stars are not significant ultraviolet sources.

3 ANALYSIS AND DISCUSSION

3.1 Atmospheric parameters

First, we constrain the effective temperature $(T_{\rm eff})$ and the surface gravity $(\log g)$. Two separate measurements show a slight systematic difference in $\log g$. Fitting the low-dispersion ${\rm H}\alpha$ to H9 profiles we measure $T_{\rm eff}=20880\pm240$ and $\log g=7.84\pm0.04$, while fitting the high-dispersion ${\rm H}\beta$ to H8 we measure $T_{\rm eff}=20890\pm140$ and $\log g=7.93\pm0.03$. Table 2 lists the weighted averages. The error bars for the surface gravity were extended in order to encompass both of our measurements. We computed the corresponding mass, age, and absolute V magnitude using the mass-radius relations of Benvenuto & Althaus (1999) with a carbon/oxygen core, thick hydrogen layer ($\log M_{\rm H}/M_*=-4$), and zero metallicity. Finally we estimated the distance using the photometric parallax method. Figure 1 shows the analysis of the low-dispersion Balmer line profiles.

Next, we calculated the space motion of the star using the proper-motion (Third U.S. Naval Observatory CCD Astrograph Catalog) and the barycentric velocity (see Table 3) corrected for the gravitational redshift ($\gamma_g = 25.9^{+1.3}_{-2.4}$), $v_{\rm bary,corr} = 12.5$ km s⁻¹. We employed the methodology described by Johnson & Soderblom (1987) and the solar motion from Hogg et al. (2005). The star belongs to the thin disc population.

Our basic model atmosphere grid was computed in local thermodynamic equilibrium (LTE), but additional non-LTE model atmospheres were computed using TLUSTY (Hubeny & Lanz 1995; Lanz & Hubeny 1995). We determined the non-LTE metallicity vector by fitting a non-LTE model at 20900 K and $\log g = 7.9$ to a grid of pure-hydrogen

Table 2. Properties of the DAZ GALEX J1931+0117

Parameter	Measurement
Effective temperature Surface gravity Mass Absolute magnitude Cooling age	$\begin{split} T_{\rm eff} &= 20890 \pm 120 \text{ K} \\ \log g &= 7.90^{+0.03}_{-0.06} \text{ (c.g.s.)} \\ M &= 0.57^{+0.02}_{-0.03} M_{\odot} \\ M_{V} &= 10.50^{+0.05}_{-0.10} \\ t_{\rm cool} &= 4.5 \pm 0.6 \times 10^{7} \text{ yrs} \end{split}$
Distance Kinematics	$d = 55^{+5}_{-3} \text{ pc} (U, V, W) = (28, 5, 22) \text{ km s}^{-1}$

Table 3. UVES line identification

Ion	$\lambda \ ({A})$	E.W. (mÅ)	$v_{\rm bary}^{\ a}$ (km s ⁻¹)
Si II	3853.660	17.	36.6
Si II	3856.020	56.	36.8
Si 11	3862.609	50.	36.7
Ca II	3933.663	50.	37.1
Ca II	3968.469	11.	37.7
Si II	4128.070	56.	36.4
Si 11	4130.890	83.	36.2
Mg II	4481.13/.33	579.	33.7
Fe II	4549.474	6.	35.3
Si III	4552.622	11.	38.1
Fe II	4923.927	12.	37.6
Si 11	5957.560	34.	40.8
Si II	5978.930	49.	43.2
Si 11	6347.100	132.	36.4
Si II	6371.360	102.	36.4
Οı	7771.944	39.	39.2
Οı	7774.166	31.	39.0
Οı	7775.388	22.	41.5
Mg II	7877.054	46.	45.5
Mg II	7896.366	103.	45.5
Сап	8542.091	18.	35.8

 $[^]a$ Average barycentric velocity $v_{\rm bary} = 38.4 \pm 3.2 \ \rm km \ s^{-1}.$

LTE models. We measured $\Delta T_{\rm eff} = +120$ K and $\Delta \log g = -0.04$. We conclude that despite the high-metallicity of the atmosphere, the systematic error introduced by using pure-H LTE models is within statistical errors.

3.2 Photospheric abundances and diffusion

Table 3 lists the heavy-element lines identified in the UVES spectra. The average barycentric velocity of the trace elements ($v_{\rm bary}=38.4\pm3.2~{\rm km~s^{-1}}$) is in agreement with the H α velocity $v_{\rm H}\alpha=37.6\pm0.8~{\rm km\,s^{-1}}$. We determined the photospheric abundances by fitting the observed line profiles with non-LTE models. Figure 2 shows selected heavy element line profiles and best-fit models. We did not notice line splitting due to a magnetic field at the resolution limit ($R=\lambda/\Delta\lambda\approx40,000$). Since $\Delta\lambda/\lambda=4.7\times10^{-7}\lambda\,B$ where λ is in Å and B in MG, the limit implied is $B\lesssim10~{\rm kG}$.

Table 4 lists the measured abundances. Helium and carbon are not detected and we employed He I λ 5875.7 and C II λ 4267.001-183 to set abundance upper limits. The infrared calcium triplet region shows weak photospheric absorption but no gaseous disc emission with a limit of $E.W. \leq$

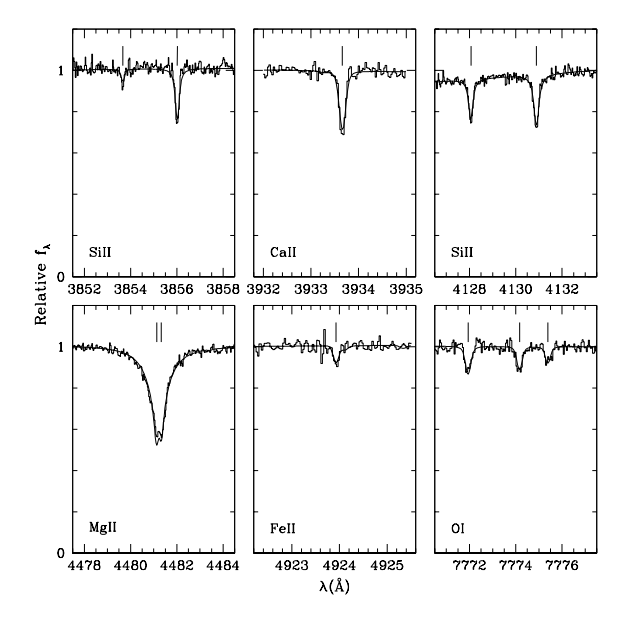


Figure 2. Echelle spectra (UVES) of the DAZ GALEX J1931+0117 showing a strong Mg doublet and weaker oxygen, silicon, calcium and iron lines.

1Å. The abundance of magnesium in GALEX J1931+0117 exceeds that of SDSS J122859.93+104032.9 by a factor of 5 but no evidence of a gaseous disc is found in disagreement with a correlation between magnesium abundance and calcium emission strength in hot DAZ white dwarfs found by Gänsicke, Marsh, & Southworth (2007). However, Jura (2008) argues that gaseous discs are rare and that in the two cases discussed by Gänsicke, Marsh, & Southworth (2007) an additional source of heating must be responsible for this unusual phenomenon.

The near-solar heavy element abundance in the atmosphere of GALEX J1931+0117 must be supplied from an external source. The accreted material reaches optical depth unity, $\tau_R \approx 1$, and, assuming near steady-state, appears in the optical spectra at the measured abundances, n(X)/n(H). The elements are supplied in the accretion flow in proportions $n(X)/n(H)_{flow}$ that are not necessarily solar. The steady-state abundances are proportional to (1) the supplied abundances and (2) their respective diffusion time-scales. For example, the measured abundance of element X relative to silicon is given by

$$\frac{n(\mathbf{X})}{n(\mathbf{Si})} = \frac{\tau(\mathbf{X})}{\tau(\mathbf{Si})} \frac{n(\mathbf{X})}{n(\mathbf{Si})}_{\text{flow}}$$
(1)

where the time-scale $\tau(X)$ is given at a selected point in the atmosphere by

$$\tau(X) = \frac{m}{\rho v} \tag{2}$$

where m is the column mass density (g cm⁻²), ρ is the local mass density (g cm⁻³), and v is the diffusion velocity (cm s⁻¹) at that point. These quantities are calculated at $\tau_R = 1$. Both m and ρ are provided by the model atmosphere. The diffusion velocity $v = v(T, n_p, X_i)$ is calculated following the prescription of Fontaine & Michaud (1979) in a fully ionized hydrogen gas ($Z_{\rm H} = 1$), and the remaining vari-

ables, temperature T, proton density n_p , and the ionization fractions X_i of element X are also provided by the model atmosphere. The diffusion velocity is averaged over all ionization species following Montmerle & Michaud (1976). The relatively high concentrations of neutral helium and oxygen contribute toward shorter diffusion time scales compared to elements with lower concentrations of neutral species.

Table 4 summarises our calculations. Using Equation (1) we calculated the abundances relative to silicon that are required in the accretion flow to reproduce the observed abundance ratios and compared them to solar ratios.

Again, assuming steady state accretion, the total mass of element X accreted per year and mixed into an atmosphere of mass $M=4\pi R^2\,m$, where R is the white dwarf radius, is given by

$$\dot{M} = A(X) \frac{n(X)}{n(H)} \frac{4\pi R^2 m}{\tau(X)}$$
(3)

where $A({\rm X})$ is the atomic weight of element X and the abundance is given relative to the main constituent. For example, magnesium and silicon must be accreted at a rate of 4×10^{15} and 6×10^{15} gyr $^{-1}$, respectively. The total accretion rate for magnesium and silicon is well within the range predicted by the tidal destruction of asteroids (Jura 2008), but the relatively low abundance of calcium argues against this scenario. Abundance measurements in the dusty helium-rich white dwarfs GD 40 (Klein et al. 2010) and GD 362 (Koester 2009), and hydrogen-rich white dwarf G 29-38 (Koester 2009) imply a calcium-rich accretion flow with $n({\rm Ca})/n({\rm Mg})\sim 0.1-1$. The accretion flow in GALEX J1931+0117 is low in calcium $(n({\rm Ca})/n({\rm Mg})\sim 0.02)$, somewhat below the solar ratio. Within uncertainties the accretion flow has near solar composition.

Alternatively, assuming that the accreted material is supplied by mass loss from a low-mass companion, the accreted mass of the main constituent (hydrogen) is scaled on the accreted mass of trace elements. Averaging the observed variations between elements, the total accretion rate is estimated at $\dot{M}_{\rm acc} = 3 \times 10^{-14} \, M_{\odot} \, {\rm yr}^{-1}$. Using the post-common envelope white dwarf plus brown dwarf binary WD0137-349 as an example we arbitrarily locate a L5 companion (see section 3.3) of $0.05 M_{\odot}$ (see Kirkpatrick 2005) at a separation of $a = 1 R_{\odot}$. The fraction of material captured by the white dwarf would then dictate the required mass-loss rate for the companion. Assuming in turn a geometrical crosssection, a gravitationally-focused cross-section, or fluid accretion (Wesemael, Henry, & Shipman 1984; Debes 2006), the fraction is estimated at 5×10^{-5} , 3×10^{-3} , or 0.02-0.08, respectively. Under the assumption of fluid accretion, the required mass-loss rate is $\dot{M}_{\rm acc} = 0.4 - 1.5 \times 10^{-12} \, M_{\odot} \, {\rm yr}^{-1}$. This rate exceeds the solar rate or the upper limit derived for Proxima Centauri implying that mass loss may be stimulated by tidal or irradiation effects in a close binary (see a discussion by Debes 2006).

3.3 Infrared excess: low-mass star or dusty disc

Figure 3 compares the spectral energy distribution from the UV to the NIR to computed composite spectra. Adopting class averages of $M_J = 12.0, 13.0, 13.5$, and 14.0 for L2, L4, L5, and L6, respectively (Kirkpatrick 2005), we scaled corresponding L templates from the IAC M-L-T Dwarf Catalog

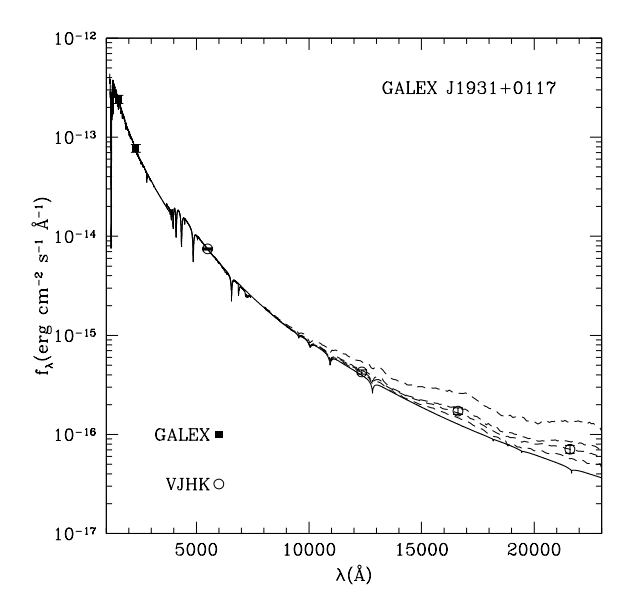


Figure 3. UV to NIR spectral energy distribution based on *GALEX* FUV and NUV photometry, the NTT V magnitude, and 2MASS JHK photometry compared to a white dwarf model (full line). Contributions from (top to bottom dashed lines) a L2, L4, L5, and L6 dwarf are added to the white dwarf model.

(Martín, Cabrera, & Cenizo 2005) to a distance of 55 pc, and added the flux to the projected NIR continuum of the DAZ white dwarf. The measured excess would correspond to a L5 dwarf with $T_{\rm eff}\sim 1700$ K (Kirkpatrick 2005).

Assuming $M_2=0.05\,M_\odot$ and $a=1\,R_\odot$, the predicted L5 and DAZ velocity semi-amplitudes are $K_{\rm L5}=314\cdot\sin i\,$ km s⁻¹ and $K_{\rm DAZ}=28\cdot\sin i\,$ km s⁻¹, respectively. Radial velocity shifts in the white dwarf spectra may be detectable in future observations. The presence of a close L dwarf companion should lead to notable optical/infrared light variations. In particular, variable H α emission is a noted spectroscopic signature of post-common envelope systems (e.g., WD0137–349, Maxted et al. 2006), but it is not apparent in any of our spectra.

We cannot exclude the presence of a dusty circumstellar environment in addition to a L dwarf companion. However, by showing a steeper decline over the H- and K-bands the NIR spectral energy distribution of GALEX J1931+0117 appears different than that of the warm, dusty white dwarf SDSS J122859.93+104032.9 (Brinkworth et al. 2009). If present, dust should reside at a distance from the star where the equilibrium temperature between dust and stellar radiation is below the sublimation temperature, $T_{\rm sub}$ (see Jura 2008). For $T_{\rm sub}$ between 1350 and 1650 K (see Lodders 2003) the minimum distance from GALEX J1931+0117 or SDSS J122859.93+104032.9 is between 1.7 and 1.1 R_{\odot} . In fact, Brinkworth et al. (2009) found that the gaseous and dusty discs in SDSS J122859.93+104032.9 co-exist at a distance $\lesssim~1.2\,R_\odot$ from the white dwarf. Although GALEX J1931+0117 and SDSS J122859.93+104032.9 have nearly identical luminosities, the lack of a gaseous disc in the former and the dissimilarity of their NIR spectral energy distributions imply different environments.

Table 4. Photospheric abundances

X	$n(\mathbf{X})/n(\mathbf{H})$	n(X)/n(Si)	$n(X)/n(Si)_{\odot}$ ^a	$\tau(\mathrm{Si})/\tau(\mathrm{X})^{\ b}$	$n(X)/n(Si)_{flow}$ ^c	Departure from solar^d
Не	$< 5 \times 10^{-4}$	< 7.8	2.6×10^{3}	60.	$\lesssim 5 \times 10^2$	$\lesssim 0.2$
$^{\mathrm{C}}$	$< 7 \times 10^{-5}$	< 1.1	7.6	1.07	$\lesssim 1.2$	$\lesssim 0.2$
O	$2.4 \pm 0.2 \times 10^{-4}$	3.8 ± 0.4	14.	7.4	~ 30	~ 2
Mg	$7.1 \pm 0.3 \times 10^{-5}$	1.1 ± 0.1	1.1	0.81	~ 0.9	~ 0.8
Si	$6.4 \pm 0.3 \times 10^{-5}$	•••	•••		***	•••
Ca	$9.0 \pm 1.8 \times 10^{-7}$	0.014 ± 0.003	0.063	1.23	~ 0.02	~ 0.3
Fe	$2.9 \pm 0.6 \times 10^{-5}$	0.45 ± 0.09	0.87	1.86	~ 0.8	~ 1

^a Abundances in the solar photosphere from Grevesse, Asplund, & Sauval (2007). ^b Ratio of diffusion time scales at $\tau_R = 1$.

4 SUMMARY AND CONCLUSIONS

We identified and analysed the properties of one of the most heavily polluted white dwarfs known. The source of the material remains unknown, although the measured NIR excess may be attributed to a L5 dwarf or to a warm debris disc. The measured abundances suggest that the material is accreted onto the atmosphere in solar proportions and favour a model involving a L dwarf companion in a close orbit. However, the $H\alpha$ emission notable in such systems is absent in GALEX J1931+0117 and the mass loss imposed on the companion appears excessive. NIR intermediate dispersion spectroscopy should help determine the nature of the accretion source. Additional optical spectra will be useful to trace putative orbital motions while Space Telescope Imaging Spectrograph high-dispersion spectra will be useful to constrain further the carbon abundance and extend the pattern to less abundant elements.

ACKNOWLEDGMENTS

S.V. and A.K. are supported by GA AV grant numbers IAA300030908 and IAA301630901, respectively, and by GA ČR grant number P209/10/0967. A.K. also acknowledges support from the Centre for Theoretical Astrophysics (LC06014). We thank the referee for useful suggestions. This publication makes use of data products from the Two Micron All Sky Survey, which is a joint project of the University of Massachusetts and the Infrared Processing and Analysis Center/California Institute of Technology, funded by the National Aeronautics and Space Administration and the National Science Foundation.

REFERENCES

Abazajian K. N., et al., 2009, ApJS, 182, 543

Alcock C., Fristrom C. C., Siegelman R., 1986, ApJ, 302, 462

Benvenuto O. G., Althaus L. G., 1999, MNRAS, 303, 30 Brinkworth C. S., Gänsicke B. T., Marsh T. R., Hoard D. W., Tappert C., 2009, ApJ, 696, 1402

Burleigh M. R., Hogan E., Dobbie P. D., Napiwotzki R., Maxted P. F. L., 2006, MNRAS, 373, L55

Debes J. H., 2006, ApJ, 652, 636

Debes J. H., Sigurdsson S., Woodgate B. E., 2005, AJ, 130, 1221

Farihi J., Jura M., Zuckerman B., 2009, ApJ, 694, 805

Fontaine G., Michaud G., 1979, ApJ, 231, 826

Gänsicke B. T., Marsh T. R., Southworth J., 2007, MN-RAS, 380, L35

Gänsicke B. T., Marsh T. R., Southworth J., Rebassa-Mansergas A., 2006, Sci, 314, 1908

Grevesse N., Asplund M., Sauval A. J., 2007, SSRv, 130, 105

 $Hogg\ D.\ W.,\ Blanton\ M.\ R.,\ Roweis\ S.\ T.,\ Johnston\ K.\ V.,\ 2005,\ ApJ,\ 629,\ 268$

Holberg J. B., Barstow M. A., Green E. M., 1997, ApJ, 474, L127

Hubeny I., Lanz T., 1995, ApJ, 439, 875

Johnson D. R. H., Soderblom D. R., 1987, AJ, 93, 864Jura M., 2008, AJ, 135, 1785

Kawka A., Vennes S., Dupuis J., Chayer P., Lanz T., 2008, ApJ, 675, 1518

Kilic M., Redfield S., 2007, ApJ, 660, 641

Kirkpatrick J. D., 2005, ARA&A, 43, 195

Klein B., Jura M., Koester D., Zuckerman B., Melis C., 2010, ApJ, 709, 950

Koester D., 2009, A&A, 498, 517

Koester D., Rollenhagen K., Napiwotzki R., Voss B., Christlieb N., Homeier D., Reimers D., 2005, A&A, 432, 1025

Lanz T., Hubeny I., 1995, ApJ, 439, 905

 $Lodders\ K.,\ 2003,\ ApJ,\ 591,\ 1220$

Martín E. L., Cabrera J., Cenizo E., 2005, AN, 326, 1026 Maxted P. F. L., Napiwotzki R., Dobbie P. D., Burleigh M. R., 2006, Nature, 442, 543

Montmerle T., Michaud G., 1976, ApJS, 31, 489

Morrissey P., et al., 2007, ApJS, 173, 682

Ochsenbein F., Bauer P., Marcout J., 2000, A&AS, 143, 23 Schlegel D. J., Finkbeiner D. P., Davis M., 1998, ApJ, 500, 525

Skrutskie M. F., et al., 2006, AJ, 131, 1163

Steele P. R., Burleigh M. R., Farihi J., Gänsicke B. T., Jameson R. F., Dobbie P. D., Barstow M. A., 2009, A&A, 500, 1207

Vennes S., Kawka A., Németh P., 2010, in preparation Wesemael F., Henry R. B. C., Shipman H. L., 1984, ApJ, 287, 868

Zuckerman B., Koester D., Melis C., Hansen B. M., Jura M., 2007, ApJ, 671, 872

Zuckerman B., Koester D., Reid I. N., Hünsch M., 2003, ApJ, 596, 477

^c Predicted abundance ratio in the accretion flow. ^d Predicted abundance ratio in the accretion flow relative to solar.